

# Electron spin-orbit interaction in helically coiled carbon nanotube

Ning Ma<sup>1,2†</sup>, Daqing Liu<sup>2</sup>, Vei Wang<sup>2,3</sup>, Erhu Zhang<sup>2</sup>, Shengli Zhang<sup>2\*</sup>

<sup>1</sup>Department of Physics, MOE Key Laboratory of Advanced Transducers and Intelligent Control System, Taiyuan University of Technology, Taiyuan 030024, China

<sup>2</sup>Department of Applied Physics, MOE Key Laboratory for Nonequilibrium Synthesis and Modulation of Condensed Matter, Xi'an Jiaotong University, Xi'an 710049, China

April 5, 2019

## Abstract

Recent theoretical and experimental works on carbon nanotubes (CNTs) have revealed that spin-orbit interaction (SOI) is more robust than it was thought. Motivated by this, we investigate the SOI in helically coiled CNTs. Calculations are performed within the tight-binding model with the inclusion of a four-orbital basis set; thereby the full symmetry of the helical lattice and the hybridization of  $\pi$  and  $\sigma$  bands are considered. By virtue of unitary transformation and perturbation approach, we obtain the analytic solution for the torsion-dependent SOI in helically coiled CNTs. Due to the enhancement of curvature and torsion, the calculated SOI values reach the order of meV which has been confirmed by *ab initio* electronic structure calculation.

PACS numbers: 73.63.Fg, 71.70.Ej, 73.22.-f

## 1 INTRODUCTION

Carbon nanotubes (CNTs) have been the focus of intense study in the past few decades as they exhibit remarkable properties that make them good candidates for molecular electronic devices.<sup>1</sup> Lately CNTs spintronics, by combining electronics with spintronics to inject, detect, and manipulate the electron spin in CNTs systems, has been gradually regarded as one of the most promising research fields.<sup>2–4</sup> Meanwhile their application as building blocks in spintronics has been also addressed.<sup>5–8</sup> Nonetheless, the spin-orbit interaction (SOI) has been customarily underestimated in CNTs,<sup>9</sup> due to the low atomic number of carbon ( $Z = 6$ ). Only recently was it proven experimentally<sup>10</sup> that in the spectrum of ultraclean straight carbon nanotubes (SCNTs), the effects of this coupling between spin and orbital degrees of freedom are clearly visible. This observation is in agreement with previous theoretical predictions,<sup>11–13</sup> which argued that SOI could be significant in SCNTs due to their curvature. Understanding the effects of this coupling is essential for the successful manipulation of the different degrees of freedom of these systems, thereby affecting the transport properties of electrons, so it's a crucial issue in condensed matter physics and spintronics. To date, the spin manipulation via SOI has been extensively studied in SCNTs.<sup>14–22</sup>

Motivated by this, we further explore the SOI effects in the curved CNTs. In fact, some curved CNTs (i.e. ring closure and coil-shaped CNTs, etc) have already been founded in experiment.<sup>23,24</sup> Particularly, the helically coiled carbon nanotubes (HCCNTs) firstly predicted by Ihara, Itoh, and Kitakami,<sup>25</sup> possess nonzero curvature and torsion with two kinds of disclinations (5-membered rings and 7-membered rings), but they are absent in the simple SCNTs.<sup>26,27</sup> Because of their potential applications for nano-electronic devices and nano-electromechanical systems, the HCCNTs have been attracting extensive interest.<sup>28–30</sup> Regrettably, these researches have just focused on the electronic properties without involving the spintronic properties. Especially, the law of additional SOI induced by the distortion of HCCNTs and its influence on the movement of electron, remain poorly understood. Some other critical problems should be also thoroughly investigated, such as the chirality how to affect the SOI? Does the SOI revised by the torsion have any of the new physical effect? The most interesting target raised for us is to clarify the role of SOI in such nanostructures. However, because of its complicated configuration, the analytical calculations for SOI becomes an extremely challenging issue. These researches have important academic significance on the design of new mesoscopic spin electronic device.

In this paper, we calculate the SOI in HCCNTs by employing the perturbation theory and the tight binding approximation for nearest-neighbor hopping. These methods have been well applied to an infinite graphene and a carbon nanotube, etc.<sup>13</sup> In Ref. 13, Guinea *et al.* take two atoms of equal height along the axis of the tube (i.e. the Armchair-SCNT) as the model, and obtain the SOI with the angle  $\theta$ , in the limit when the radius of curvature is much longer than the interatomic spacing,  $a \ll R$ , is given by  $\theta \approx a/R$ . Here we start from a more general case as two atoms of different height (i.e. the Chiral-SCNT), and recover the angle  $\theta$  including the chiral angle  $\psi_c$  without the limit condition above, and on this basis, we can further clarify the chiral effect on the HCCNT's SOI. To accomplish this, we introduce an unitary matrix  $\mathbf{U}$ , which has bridged the coordinates between SCNT and HCCNT. By virtue of the  $\mathbf{U}$  matrix, we derive the analytical solution  $\xi_R$  of SOI, and find the  $\xi_R$  for the  $\pi$  bands is first order in the atomic carbon SOI strength  $\xi_0$  (i.e.  $\xi_R \propto \xi_0$ ), similar to the ‘‘Rashba-type’’ SOI in graphene.<sup>13,31</sup> But strikingly different from graphene and SCNT, the term  $\xi_R$  largely depends on both the curvature  $\kappa$  and the torsion  $\tau$ . Due to their enhancement, the calculated SOI values reach the order of  $meV$ . To check the validity of  $\xi_1$ , we specially compute five different *ab initio* energies of SOI for five different HCCNTs of coiled pitch  $p_s$ , and verify the theoretical estimated SOIs, qualitatively and quantitatively, agree well with realistic *ab initio* calculation values.

This paper is organized as follows. In section 2, a brief introduction is given to the details of calculation methods. Finally, we derive the analytic solution of SOI. In section 3, *ab initio* calculations are described, and the results compared with analytic solutions are discussed. In the last section, we present brief summary and conclusions.

## 2 GENERAL SOLUTION

In graphene, the carbon atoms are arranged into a hexagonal lattice connected by strong covalent bonds of  $\sigma$ -orbitals derived from the  $sp^2$  hybridization of the atomic orbitals. The remaining  $p_x$  orbital (normal to the atomic plane) has a weak overlap and forms a narrow band of  $\pi$ -orbitals states. To a first approximation, the  $\pi$ -electron system can be modeled as a tight-binding Hamiltonian characterized by a single hopping matrix element between neighboring atoms, and the energy offset of the  $p$ -electron states. Considering the arbitrary atom of pentagon–heptagon pairs in HCCNTs is still surrounded by three nearest neighbor atoms similar to the hexagon case, we reasonably choose the tight-binding model with a two-center Slater-Koster approximation<sup>32</sup> for nearest-neighbor hopping in our calculations. The tight-binding representation of Hamiltonian is defined by the combination of the contributions  $H_0$  and  $H_{SO}$ ,

$$H = H_0 + H_{SO}. \quad (1)$$

Here, the spin-independent noninteracting Hamiltonian reads  $H_0 = \sum_{i\mu s'} c_{i\mu s'}^\dagger t_{i\mu} c_{i\mu s'} + \sum_{\langle i\mu s', j\mu' s' \rangle} c_{i\mu s'}^\dagger t_{i\mu, j\mu'} c_{j\mu' s'}$ , where  $\langle i, j \rangle$  is a shorthand used to denote neighboring atomic sites,  $\langle \mu, \mu' \rangle$  refers to the  $s$  and  $p_x, p_y, p_z$  atomic orbitals on each site, and  $s' = \uparrow, \downarrow$  the electronic spin. The term  $t_{i\mu}$  stands for the ‘‘on-site’’ atomic energies of  $2s$  and  $2p$  orbitals, i.e. the site-diagonal matrix elements  $t_{is}$  and  $t_{ip}$ , with the latter one  $t_{ip} = 0$ . Besides, the Wannier representation of  $H_0$  describes electrons hopping from  $j$  atom to another,  $i$ . The strength of the hopping matrix element  $t_{i\mu, j\mu'}$  is controlled by the effective overlap of neighboring atoms. The tight-binding representation becomes useful when the  $t_{i\mu, j\mu'}$  is non-vanishing, but the orbital overlap is so weak that only nearest-neighbor hopping effectively contributes. Here we use one parameter  $V_{pp}^\pi$  for the nearest-neighbor hopping between the  $p_x$  orbitals of the  $\pi$  band, and other parameters of  $V_{pp}^\sigma, V_{sp}^\sigma$ , and  $V_{ss}^\sigma$  for the rest of the intra-atomic hoppings between the atomic orbitals  $s, p_x, p_y$  of the  $\sigma$  band. The SOI arises  $H_{SO} = \xi_0 \mathbf{L} \cdot \mathbf{s}$ ,<sup>33,34</sup> with the intra-atomic SOI constant  $\xi_0$ , the total atomic angular momentum operator  $\mathbf{L} = \mathbf{r} \times \mathbf{p}$ , and the total electronic spin operator  $\mathbf{s}$ .

Following the approach of Ando<sup>11</sup> and Guinea<sup>13</sup> *et al.*, we analyse the hopping between the  $p_x$  and  $p_y$  orbitals in the  $\pi$  and  $\sigma$  bands for SCNT (see Fig. 1). Here we assume that the  $p_x$  orbitals are oriented normal to the surface, the  $p_y$  orbitals tangent to the surface circumference, and the  $p_z$  orbitals parallel to the tube axes. Comparing to graphene, the curvature modifies the hopping for the  $p_{x(y)}$  orbitals between the two neighboring atoms, but not changes the hopping between  $p_z$  orbitals, so the effective projections should be oriented along

$p_x$  and  $p_y$  except of  $p_z$ . Hence, the revised  $p_x$ - $p_y$  hopping Hamiltonian is given by

$$\begin{aligned}
H_h = & \sum_{s'} [V_{pp}^\pi \cos^2 \theta + V_{pp}^\sigma \sin^2 \theta] c_{x1s'}^\dagger c_{x0s'} \\
& - \sum_{s'} [V_{pp}^\pi \sin^2 \theta + V_{pp}^\sigma \cos^2 \theta] c_{y1s'}^\dagger c_{y0s'} \\
& + V_{sp}^\sigma \sin^2 \theta c_{x1s'}^\dagger c_{s0s'} + \sin \theta \cos \theta (V_{pp}^\pi - V_{pp}^\sigma) \\
& \times (c_{x1s'}^\dagger c_{y0s'} - c_{y1s'}^\dagger c_{x0s'}) + H.c.,
\end{aligned} \tag{2}$$

in which 0 and 1 denote the two neighboring atoms considered. Strikingly different from the case [see Fig. 1 (a)] in Ref. 13, we take into account two atoms of different height [see Fig. 1 (b)], and give the angle  $\theta$  between the adjacent  $p_x$  axes [see Fig. 1 (c)], with comprising the chiral angle  $\psi_c \in [0, 30^\circ]$  for the following expression,

$$\begin{cases} \sin \theta = \frac{a}{\sqrt{a^2 + (R/\cos \psi_c)^2}}, \\ \cos \theta = \frac{(R/\cos \psi_c)}{\sqrt{a^2 + (R/\cos \psi_c)^2}}, \end{cases} \tag{3}$$

where the symbols of  $a$  and  $R$ , respectively, represent the lattice spacing and the tube radius. Eq. (3) could help us to further discuss the chiral effects on the SOI.

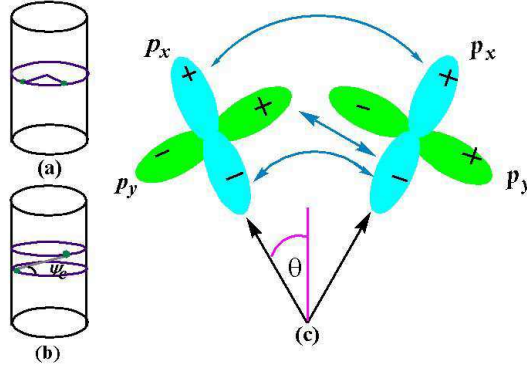


FIG. 1. (Color online) Schematic representation of the curvature effect on the transfer integrals between the orbitals of two nearest-neighbor atoms of (a) equal height and (b) different height in SCNT. (c) The  $p_x$  orbitals are not parallel anymore, so that a mixing with the orbitals  $p_y$  building the  $\sigma$  bonds takes place. The blue arrows stand for the different hoppings described in the text.

The Hamiltonian of Eq. (2) actually demonstrates the transition of  $p_x$ - $p_y$  orbitals in SCNT with the coordinate of  $(x, y, z)$ , but not in HCCNT with  $(x', y', z')$ . Aiming at this problem, we make an ansatz, that there exists a unitary matrix  $\mathbf{U}$  enables us to replace the  $(x, y, z)$  with the  $(x', y', z')$  in Eq. (2):

$$(c_x, c_y, c_z)^T = \mathbf{U} (c'_x, c'_y, c'_z)^T, \tag{4}$$

thereby leading to an transformation of the  $H_h$  from SCNT to HCCNT, which is undoubtedly the crucial step in our calculations. Thereafter, through analysing the connection between the coordinate transformation and the topological structure as illustrated in Fig. 2, we find out the matrix  $\mathbf{U}$  as

$$\mathbf{U} = \begin{pmatrix} \cos \alpha_1 \cos \beta_1 & -\cos \alpha_2 \sin \beta_2 & -\sin \phi \cos \left( \frac{\pi}{4} + \eta \right) \\ -\cos \alpha_1 \sin \beta_1 & \cos \alpha_2 \cos \beta_2 & -\sin \phi \sin \left( \frac{\pi}{4} + \eta \right) \\ \sin \alpha_1 & \sin \alpha_2 & \cos \phi \end{pmatrix}, \tag{5}$$

where the  $3 \times 3$  matrix  $\mathbf{U}$  obeys  $\mathbf{U}\mathbf{U}^\dagger = \mathbf{U}^\dagger\mathbf{U} = \mathbf{I}$  and all parameters are denoted in Fig. 2. Specifically, the process of  $\mathbf{U}$  transformation consists of two operations, i.e., around the dash line and the axis  $z$ , sequentially rolling and spinning the local coordinate  $(x, y, z)$  by  $\eta$  and  $\phi$  (see Fig. 2) for the atoms previously distributing in SCNT. Ultimately, we get the local coordinate  $(x', y', z')$  for the atoms redistributing in HCCNT. Note, the axis  $z'$  is required to be tangent to the central axis of HCCNT, and the type of HCCNT is completely determined by the inclination angle of helix  $\phi$  belonging to  $[0, 90^\circ]$ , with two limits of  $0^\circ$  and  $90^\circ$ , respectively, corresponding to the straight CNTs and the torus CNTs.

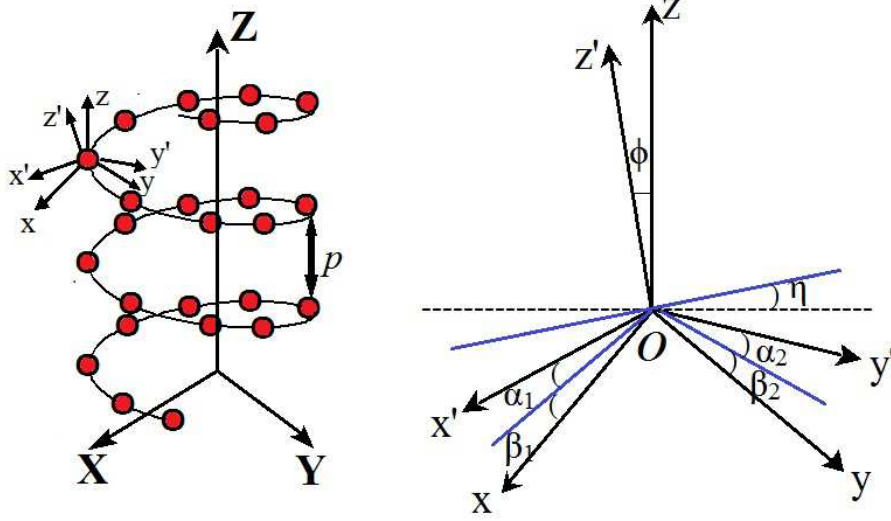


FIG. 2. (Color online) Schematic view of the coordinate transformation from the  $(x, y, z)$  of SCNT to the  $(x', y', z')$  of HCCNT. The atoms of one spiral line in HCCNT are employed to interpret the process. The fixed coordinate of  $(X, Y, Z)$ , the original local coordinate of  $(x, y, z)$ , and the final one of  $(x', y', z')$  are established on the arbitrary atom in the spiral line.

Substituting Eq. (4) into Eq. (2), and projecting onto the bloch wave functions of the  $\pi$  and  $\sigma$  bands at the  $K$  ( $K'$ ) point, we obtain the Hamiltonian of SOI for HCCNT

$$\begin{aligned}
 H_{hK(K')} &= \frac{\sqrt{6}}{4} \cos \alpha_1 \cos \alpha_2 [(V_{pp}^\pi - V_{pp}^\sigma) \sin(\beta_1 + \beta_2 - 2\theta) + (V_{pp}^\pi + V_{pp}^\sigma) \sin(\beta_2 - \beta_1)] \\
 &\times \int d^2\mathbf{r} \left\{ \cos\left(\frac{\alpha_0}{2}\right) [\Psi_{\pi AK(K')\uparrow}^\dagger(\mathbf{r}) \Psi_{\sigma 1(2)BK(K')\uparrow}(\mathbf{r}) + \Psi_{\pi BK(K')\uparrow}^\dagger(\mathbf{r}) \Psi_{\sigma 1(2)AK(K')\uparrow}(\mathbf{r})] \right. \\
 &\left. + \sin\frac{\alpha_0}{2} [\Psi_{\pi AK(K')\uparrow}^\dagger(\mathbf{r}) \Psi_{\sigma 2(1)BK(K')\uparrow}(\mathbf{r}) + \Psi_{\pi BK(K')\uparrow}^\dagger(\mathbf{r}) \Psi_{\sigma 2(1)AK(K')\uparrow}(\mathbf{r})] \right\} + H.c.,
 \end{aligned} \tag{6}$$

in which  $\Psi_{\pi(\sigma)}$  stands for the component of  $\pi$  ( $\sigma$ ) band, and the  $\alpha_0$  is determined by basic energy parameters (i.e.  $V_{ss}^\sigma$ ,  $V_{sp}^\sigma$ ,  $V_{pp}^\sigma$ , etc).<sup>13</sup> Following the unitary requiring of  $\mathbf{U}$  matrix and the approach of differential geometry,<sup>35,36</sup> we build the complicated relations to connect the angle parameters (i.e.  $\alpha$  and  $\beta$ , etc) and the characteristic parameters (i.e. curvature  $\kappa$ , torsion  $\tau$ , coiled pitch  $p = 2\pi h$ , inclination angle of helix  $\phi$ , and coil radius  $r_0$ ,

etc) as follows,

$$\begin{aligned}
\alpha_1 &= \arcsin \left[ \sin \left( \frac{\pi}{4} - \eta \right) \kappa \sqrt{h^2 + r_0^2} \right], \\
\alpha_2 &= \arcsin \left[ \sin \left( \frac{\pi}{4} + \eta \right) \kappa \sqrt{h^2 + r_0^2} \right], \\
\beta_1 &= \frac{1}{2} \left\{ \arccos \left[ \lambda \left( 1 - \frac{\cos^2 \phi}{mn} \right)^{1/2} \right] + \arccos \left( \sqrt{\frac{\cos^2 \phi}{mn}} \right) \right\} - \eta, \\
\beta_2 &= \frac{1}{2} \left\{ \arccos \left( \sqrt{\frac{\cos^2 \phi}{mn}} \right) - \arccos \left[ \lambda \left( 1 - \frac{\cos^2 \phi}{mn} \right)^{1/2} \right] \right\} + \eta,
\end{aligned} \tag{7}$$

with

$$\begin{aligned}
\phi &= \arctan \frac{r_0}{h}, \\
\eta &= \arctan \left( \frac{\sqrt{3}a}{2r_0} \cos \psi_c \right), \\
\lambda &= \frac{1 + \tau^2 (h^2 + r_0^2)}{1 - \tau^2 (h^2 + r_0^2)}, \\
m &= 1 - \sin^2 \left( \frac{\pi}{4} - \eta \right) \kappa^2 (h^2 + r_0^2), \\
n &= 1 - \sin^2 \left( \frac{\pi}{4} + \eta \right) \kappa^2 (h^2 + r_0^2).
\end{aligned} \tag{8}$$

From Eqs. (7) and (8), two realistic facts are revealed as: 1) The hopping term of Eq. (6) largely depends on the characteristic parameters; 2) The hopping term is caused by intrinsic curvature and torsion. Assuming the energies of  $\sigma$  bands are well separated from the energy of the  $\pi$  bands [ $t_\pi = 0$  at the  $K(K')$  point], we finally derive the effective Hamiltonian acting on the states of the  $\pi$  band from Eq. (6) by using second-order perturbation theory,

$$H_{\pi K(K')} = -i\xi_R \int d^2\mathbf{r} [\pm \Psi_{\pi AK(K')\uparrow(\downarrow)}^\dagger(\mathbf{r}) \Psi_{\pi BK(K')\downarrow(\uparrow)}(\mathbf{r}) \mp \Psi_{\pi BK(K')\downarrow(\uparrow)}^\dagger(\mathbf{r}) \Psi_{\pi AK(K')\uparrow(\downarrow)}(\mathbf{r})], \tag{9}$$

in which

$$\xi_R = \frac{\xi_0 V_1 \cos \alpha_1 \cos \alpha_2}{2(2V_1^2 + V_2^2)} [(V_{pp}^\pi - V_{pp}^\sigma) \sin(\beta_1 + \beta_2 - 2\theta) + (V_{pp}^\pi + V_{pp}^\sigma) \sin(\beta_2 - \beta_1)], \tag{10}$$

with  $V_1 = (t_{is} - t_{ip})/3$  and  $V_2 = (V_{ss}^\sigma + 2\sqrt{2}V_{sp}^\sigma + 2V_{pp}^\sigma)/3$ . The geometry-dependent term  $\xi_R$  demonstrate that the hopping term of Eq. (6) causes an mixing of the  $\pi$  and  $\sigma$  orbitals, thereby modifying the SOI in graphene and SCNT. This process is quite sensitive to the deformations of helical lattice along the bond direction between the different atoms where the  $p$  part of the  $sp^2$  orbitals.

Defining a  $4 \times 4$  spinor

$$\Psi_{\pi K(K')} = \begin{pmatrix} \Psi_{A\uparrow(\mathbf{r})} \\ \Psi_{A\downarrow(\mathbf{r})} \\ \Psi_{B\uparrow(\mathbf{r})} \\ \Psi_{B\downarrow(\mathbf{r})} \end{pmatrix}_{\pi K(K')}, \tag{11}$$

we rewrite Eq. (9) in the following ‘‘Rashba-type’’ interaction form:<sup>13,31,37</sup>

$$\begin{aligned}
H_{R\pi K(K')} &= -i\xi_R \int d^2\mathbf{r} \Psi_{\pi K(K')}^\dagger(\mathbf{r}) (\pm \sigma_+ \mathbf{s}_\pm \mp \sigma_- \mathbf{s}_\mp) \Psi_{\pi K(K')}(\mathbf{r}) \\
&= \frac{\xi_R}{2} \int d^2\mathbf{r} \Psi_{\pi K(K')}^\dagger(\mathbf{r}) (\sigma_x \mathbf{s}_y + \lambda_z \sigma_y \mathbf{s}_x) \Psi_{\pi K(K')}(\mathbf{r}).
\end{aligned} \tag{12}$$

Here the  $\sigma_\alpha$  Pauli matrices act in the  $A(B)$  space with  $\sigma_z$  eigenstates localized on the  $A(B)$  sublattice,  $\lambda_z = \pm 1$  describing states at the  $K(K')$  points, and the  $\mathbf{s}_\alpha$  are Pauli matrices acting on the electron’s spin.

Our results clearly show that the effective SOI  $\xi_R$  for the  $\pi$  bands is first order in the atomic carbon SOI strength  $\xi_0$ , similar to the “Rashba-type” form in graphene.<sup>13,31,37</sup> For completeness, we add the quite weak intrinsic SOI<sup>13</sup> (without considering the effects of curvature and torsion)  $\xi_{int} \simeq (3\xi^2/4V_1)(V_1/V_2)^4 \sim 1.0 \mu\text{eV}$  which has a leading contribution proportional to  $\xi^2$ . Therefore, the total SOI strength  $\xi^*$  should be further estimated by  $\xi^* = \xi_R + \xi_{int}$ . Taking five different coiled pitches  $p \sim 7.4, 7.6, 7.8, 8.1, 8.3 \text{ \AA}$ , we get the corresponding values of SOI  $\xi^* \sim 0.91, 0.93, 0.95, 0.99, 1.01 \text{ meV}$ , respectively. Strictly speaking, the geometry factors (i.e.,  $a, r_0, R$ , etc) are closely related to the coiled pitch  $p$ , and that is mean, the calculations of SOI energies for different  $p_s$  should match different factors. Whereas, the variation range of  $p$  is so small that we can neglect the differences in the  $p$ -dependent factors.

Figure 3 directly presents a positive correlation between the tight-binding SOI energies  $\xi^*$  and the torsion  $\tau$  with the given parameters above. In stark contrast to the SOI of graphene (i.e. the order of  $\mu\text{eV}$ ), the SOI  $\xi^*$  of HCCNT has been notably improved owing to the effects of curvature and torsion resulting from the structure itself.

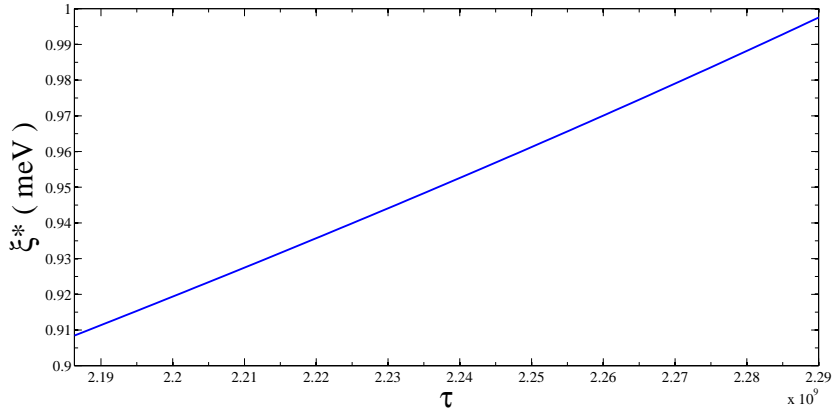


FIG. 3. The tight-binding SOI energies  $\xi^*$  of HCCNTs as a function of the torsion  $\tau$ . The  $\xi^*$  has been estimated using the parameters as  $\xi_0 = 12 \text{ meV}$  for the SOI constant of carbon;  $t_s = -7.4 \text{ eV}$ ,  $t_p = 0.0 \text{ eV}$  for the on-site energies;  $V_{ss}^\sigma = -3.63 \text{ eV}$ ,  $V_{sp}^\sigma = 4.2 \text{ eV}$ ,  $V_{pp}^\sigma = 5.38 \text{ eV}$ , and  $V_{pp}^\pi = -2.24 \text{ eV}$  for the intralayer nearest-neighbor interactions between the  $2s, 2p_x, 2p_y, 2p_z$  orbitals. Other parameters are  $V_1 = 2.47 \text{ eV}$ ,  $V_2 = 6.33 \text{ eV}$ ,  $a = 1.42 \text{ \AA}$ ,  $r_0 = 2.0 \text{ \AA}$ , and  $R = 1.7 \text{ \AA}$ .

### 3 MODEL AND *AB INITIO* CALCULATIONS

#### 3.1 Model

We construct the primitive cell of HCCNT with 120 carbon atoms ( $C_{120}^{HC}$ ) by tiling the optimized pattern of torus CNT ( $C_{120}^T$ ). Along the radius of curvature, the torus is cut into small pieces, which are stretched toward the fiber axis and combined continuously to obtain the initial atomic positions of the helical structures. Hence, the helix is created so that one pitch contains one torus. Along the outer ridge line of helices  $C_{120}^{HC}$ , fivefold rings appear to create positive curvature in the same fashion as in the corresponding toroidal structure. Besides, along the inner ridge line, sevenfold rings appear in representing negatively curved surface. Figure 4 shows an example of a helix coiled nanotube generated by the computer. *Ab initio* Molecular-dynamics simulations gives the optimal and thermodynamically stable  $C_{120}^{HC}$ .

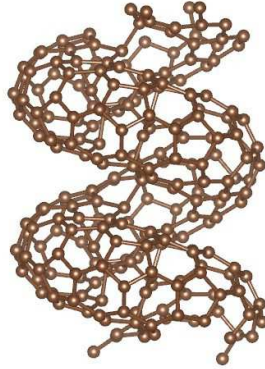


FIG. 4. (Color online) The structure of a helically coiled nanotube  $C_{120}^{HC}$  determined by *ab initio* molecular dynamics simulation (two pitch length is shown).

In present study, the helical structure of  $C_{120}^{HC}$  are left handed; however, it is possible to form right-handed helices. The optimized ground-state structure was finally derived from *ab initio* molecular-dynamics simulations with the ultrasoft pseudopotential. The two values of lowest cohesive energies per atom between helix  $C_{120}^{HC}$  and its corresponding toroidal structure  $C_{120}^T$  are almost the same: -7.37 eV, -7.39 eV, respectively. This may be due to the fact that the local and global networks of the rings of these structures are originally similar to each other. Besides, the cohesive energy of the fullerene  $C_{60}$  is -7.55 eV/atom and that of the graphite sheet is -7.44 eV/atom. These facts sufficiently demonstrate that the  $C_{120}^{HC}$  is energetically stable. In particular, using the quantum potential instead of the empirical one, we believe that the qualitative predictions mentioned below are reasonable.

### 3.2 *Ab initio* calculations

We have performed realistic *ab initio* electronic structure calculations<sup>38</sup> for  $C_{120}^{HC}$  using the projector augmented wave (PAW)<sup>39</sup> method with a Perdew–Burke–Ernzerhof (PBE) generalized gradient approximation (GGA)<sup>40</sup> density functional in order to partly test the quantitative accuracy of the conclusions reached here about SOI based on a simplified electronic structure model. The calculations were performed using VASP (Vienna Ab initio Simulation Package).<sup>41</sup> In VASP, the SOI are implemented in the PAW method which is based on a transformation that maps all electron wave functions to smooth pseudowave functions. All physical properties are evaluated using pseudowave functions.

Figure 5 compares the *ab initio* and tight-binding SOI energies with respect to the coiled pitch  $p$ . According to Eq. (10), we find that the strength of SOI approximately linearly increases with the  $p$  increasing from 7.4 to 8.3 Åm as shown with the solid (black) line. The dashed (red) line matches five different *ab initio* SOI energies for five different HCCNTs with  $p \sim 7.4, 7.6, 7.8, 8.1, 8.3$  Åm. It demonstrates that the theoretical estimated SOIs, qualitatively and quantitatively, agree well with realistic *ab initio* calculation results with the order of meV. The emergence of minor deviation between the two curves is because we neglect the tiny fluctuation of the  $p$ -dependent factors as discussed above.

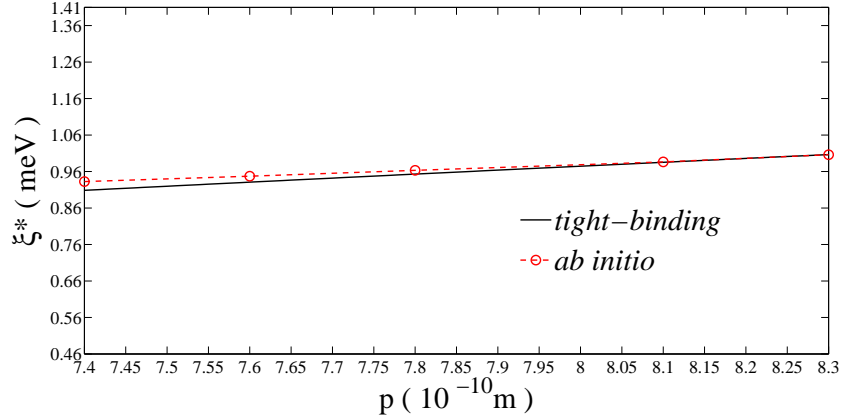


FIG. 5. (Color online) The total SOI energies of the helical structures  $\xi^*$  vs coil length of one pitch  $p$ . The solid (black) line stands for the tight-binding SOI energies, and the dashed (red) line for the *ab initio* SOI energies.

## 4 CONCLUSIONS

This paper mainly reports on a theoretical study on the SOI for HCCNTs. The SOI was treated following the approach in Refs. 11 and 13. The mixing of the  $\pi$  and  $\sigma$  bands, due to the distortion of HCCNTs, is automatically taken into account by this approach. We derived an analytic solution  $\xi_R$  for the SOI of these systems, which provides a very good matching to the numerical calculations. Following the differential geometry approach,<sup>35,36</sup> we present the relation between the  $\xi_R$  and the geometry factors (i.e. the curvature  $\kappa$  and the torsion  $\tau$ ). Because of  $\kappa$  and  $\tau$ , the value of  $\xi_R$  reaches the order of *meV*, three orders of magnitude higher than that in graphene. For completeness, we add the quite weak intrinsic SOI<sup>13</sup> (without considering the effects of curvature and torsion)  $\xi_{int} \simeq (3\xi^2/4V_1)(V_1/V_2)^4 \sim 1.0 \mu\text{eV}$  to the total SOI strength  $\xi^*$ .

## 5 ACKNOWLEDGMENTS

We thank E. H. Zhang and W. X. Zhang for insightful discussions and valuable comments on the present paper. This work is financially supported by NSF-China under Grant Nos. 11074196, 11147117, and 11305113, and by the Cultivation Fund of the Key Scientific and Technical Innovation Project, Ministry of Education of China (Grant No. 708082). We also acknowledge support from the Qualified Personnel Foundation of Taiyuan University of Technology(QPFT)(No. tyutrc-201273a).

\*Electronic address: zhangsl@mail.xjtu.edu.cn

†Electronic address: ma.ning@stu.xjtu.edu.cn

## References

- [1] S. Reich, C. Thomsen, and J. Maultzsch, *Carbon Nanotubes* (Wiley-VCH, Berlin, 2004).
- [2] C. M. Schneider, B. Zhao, R. Kozhuharova, S. Groudeva-Zotova, T. Mühl, M. Ritschel, I. Mönch, H. Vinzelberg, D. Elefant, A. Graff, A. Leonhardt, and J. Finkert, *Diamond Relat. Mater.* **13**, 215 (2004).
- [3] L. E. Hueso, J. M. Pruneda, V. Ferrari, G. Burnell, J. P. Valdés-Herrera, B. D. Simons, P. B. Littlewood, E. Artacho, A. Fert, and N. D. Mathur, *Nature (London)* **445**, 410 (2007).



- [4] C. A. Merchant and N. Markovic, Phys. Rev. Lett. **100**, 156601 (2008).
- [5] S. Sahoo, T. Kontos, J. Furer, C. Hoffmann, M. Gräber, A. Cottet, and C. Schönenberger, Nat. Phys. **1**, 99 (2005).
- [6] A. Cottet, T. Kontos, S. Sahoo, H. T. Man, M.-S. Choi, W. Belzig, C. Bruder, A. F. Morpurgo, and C. Schönenberger, Semicond. Sci. Technol. **21**, S78 (2006).
- [7] S. Koller, L. Mayrhofer, and M. Grifoni, New Journ. Phys. **9**, 348 (2007).
- [8] C. Schenke, S. Koller, L. Mayrhofer, and M. Grifoni, Phys. Rev. B **80**, 035412 (2009).
- [9] P. Avouris, Z. Chen, and V. Perebeinos, Nature Nanotechnol. **2**, 605 (2007).
- [10] F. Kuemmeth, S. Ilani, D. C. Ralph, and P. L. McEuen, Nature (London) **452**, 448-452 (2008).
- [11] T. Ando, J. Phys. Soc. Jpn. **69**, 1757 (2000).
- [12] L. Chico, M. P. López-Sancho, and M. C. Muñoz, Phys. Rev. Lett. **93**, 176402 (2004).
- [13] D. Huertas-Hernando, F. Guinea, and A. Brataas, Phys. Rev. B **74**, 155426 (2006).
- [14] D. V. Bulaev, B. Trauzettel, and D. Loss, Phys. Rev. B **77**, 235301 (2008).
- [15] H. Sun, X. L. Feng, S. Gong, and C. H. Oh, Phys. Rev. B **79**, 193404 (2009).
- [16] J. Zhou, Q. Liang, and J. Dong, Phys. Rev. B **79**, 195427 (2009).
- [17] S. H. Jhang, M. Marganska, Y. Skourski, D. Preusche, B. Witkamp, M. Grifoni, H. van der Zant, J. Wosnitza, and C. Strunk, Phys. Rev. B, **82**, 041404 (2010).
- [18] A. Schulz, A. De Martino, and R. Egger, Phys. Rev. B **82**, 033407 (2010).
- [19] T. F. Fang, Q. F. Sun, and H. G. Luo, Phys. Rev. B **84**, 155417 (2011).
- [20] M. del Valle, M. Margańska, and M. Grifoni, Phys. Rev. B **84**, 165427 (2011).
- [21] G. Kiršanskas, J. Paaske, and K. Flensberg, Phys. Rev. B **86**, 075452 (2012).
- [22] J. D. Sau and S. Tewari, Phys. Rev. B **88**, 054503 (2013).
- [23] R. Martel, H. R. Shea, and P. Avouris, Nature (London) **398**, 299 (1999).
- [24] X. B. Zhang, X. F. Zhang, D. Bernaerts, G. van Tendeloo, S. Amelinckx, J. van Landuyt, V. Ivanov, J. B. Nagy, P. Lambin, and A. A. Lucas, Europhys. Lett **27**, 141 (1994).
- [25] S. Ihara, S. Itoh, and J. I. Kitakami, Phys. Rev. B **48**, 5643 (1993).
- [26] K. Akagi, R. Tamura, M. Tsukada, S. Itoh, and S. Ihara, Phys. Rev. Lett. **74**, 2307 (1995).
- [27] P. Lambin, G. I. Márk, and L. P. Biró, Phys. Rev. B **67**, 205413 (2003).
- [28] A. Volodin, M. Ahlskog, E. Seynaeve, C. Van Haesendonck, A. Fonseca, and J. B. Nagy, Phys. Rev. Lett. **84**, 3342 (2000).
- [29] K. Hernadi, L. Thiên-Nga, and L. Forró, J. Phys. Chem. B **105**, 12464 (2001).
- [30] H. F. Hu, Y. B. Li, and H. B. He, Diamond Relat. Mater. **10**, 1818 (2001).
- [31] C. L. Kane and E. J. Mele, Phys. Rev. Lett. **95**, 226801 (2005).
- [32] J. C. Slater and G. F. Koster, Phys. Rev. **94**, 1498 (1954).
- [33] F. Guinea, J. Phys. C: Solid State Phys. **14**, 3345 (1981).

- [34] B. H. Braensden and C. J. Joachain, *Physics of Atoms and Molecules* (Addison-Wesley, New York, 1983).
- [35] O. Y. Zhong-can, Z. B. Su, and C. L. Wang, Phys. Rev. Lett. **78**, 4055 (1997).
- [36] S. Zhang, Phys. Rev. B **65**, 235411 (2002).
- [37] H. Min, J. E. Hill, N. A. Sinitsyn, B. R. Sahu, L. Kleinman, and A. H. MacDonald, Phys. Rev. B **74**, 165310 (2006).
- [38] W. Kohn and L. J. Sham, Phys. Rev. **140**, A1133 (1965).
- [39] P. E. Blöchl, Phys. Rev. B **50**, 17953 (1994).
- [40] J. P. Perdew, K. Burke, and M. Ernzerhof, Phys. Rev. Lett. **77**, 3865 (1996).
- [41] G. Kresse and J. Furthmüller, Phys. Rev. B **54**, 11169 (1996).